ISSN 0001-4370, Oceanology, 2023, Vol. 63, No. 5, pp. 719–732. © Pleiades Publishing, Inc., 2023.
Russian Text © The Author(s), 2023, published in Okeanologiya, 2023, Vol. 63, No. 5, pp. 824–839.

MARINE GEOLOGY

The article is dedicated to our colleague Boris Nikolaevich Grinko, a true friend in our marine research.

Structure of the Earth's Crust of the Persian Gulf According to Deep Seismic Sounding Results

S. A. Kovachev[a], * and O. Yu. Ganzha[a], **

[a] *Shirshov Institute of Oceanology, Russian Academy of Sciences, Moscow, Russia*

**e-mail: kovachev@ocean.ru*

***e-mail: ganja@ocean.ru*

Received June 8, 2022; revised October 11, 2022; accepted March 27, 2023

Abstract—The article presents the results of DSS seismic surveys in the Persian Gulf. Bottom analog-type seismographs and seismic airgun sources were used in the studies. The bottom seismographs were moored and shooting was carried out according to three regional profiles with a length from 100 to 250 km. The main result of these studies was a velocity–depth model of the sedimentary cover and Earth's crust up to the Moho boundary, which was revealed at a depth of about 43 km in the water area. Given that the thickness of the upper crust is only 4–5 km and based on the velocity characteristics of the remaining layers, the type of crust can be attributed to the subcontinental Archean type. This situation (complete absence or drowning of the upper layer of the Earth's crust) is typical of the waters closest to the Persian Gulf: the Black, Caspian, Mediterranean, and Red seas. A structure was found in the Earth's crust of the studied area, which may be a brachyanticline with an isometric dome-shaped shape, which corresponds to the platform-type folding in the areas of salt dome tectonics. No faults have been found in the crust of the water area of the Persian Gulf adjacent to the Bushehr Peninsula.

Keywords: Persian Gulf, deep seismic sounding, velocity section of crust, bottom seismograph

DOI: 10.1134/S0001437023050053

INTRODUCTION

Elements of the Tectonics of the Persian Gulf and Zagros Mountains

According to [43] and other authors, the Persian Gulf and Zagros mountain belt framing it from the northeast were formed as a result of collision of Arabia and microplates of Central Iran after closing of the Neotethys Ocean. The time of the initial collision along the Zagros Mountains ranges from the Late Cretaceous to the Pliocene [26, 29]. In some studies, Zagros was considered an example of a young continent, a continental collisional belt [30, 31].

In the Arabia–Eurasia collision zone, according to [27, 35, 48], orogenic plateaus formed as a result of a continent–continent collision, as evidenced by the Turkish–Iranian Highlands. Plateaus form during continental collisions, where crustal thickening and surface uplift are combined with relatively slow erosion and incision rates that limit further thickening and landform formation [37]. This is true for the Persian Gulf.

The boundaries of the Zagros–Persian Gulf collision zone are clearly delineated by topographic and seismological characteristics [36]. Sharp topographic fronts in the Persian Gulf and along the northern side of the Greater Caucasus and Kopetdag delineate the southern and northern margins of large active deformations in the area.

According to [24, 49], subduction of the Arabian Plate under Zagros, which occurred in the Vendian, was gradually replaced by collision. There are four zones in the Zagros Fars segment (Fig. 1): Imbricated, High Zagros, Low Zagros, and Piedmont. According to the proposed interpretation of the evolution of the Zagros, collisional compression in the zone of the Main Thrust led to the appearance of gentle folds in front of it in the Imbricated Zone, similar to those now developing in the Piedmont Zone. The folds were directly reflected in the relief and, during weathering, served as a source of detrital material [24, 49]. Fars is separated from Dezful province by the Kazerun fault zone (Fig. 1).

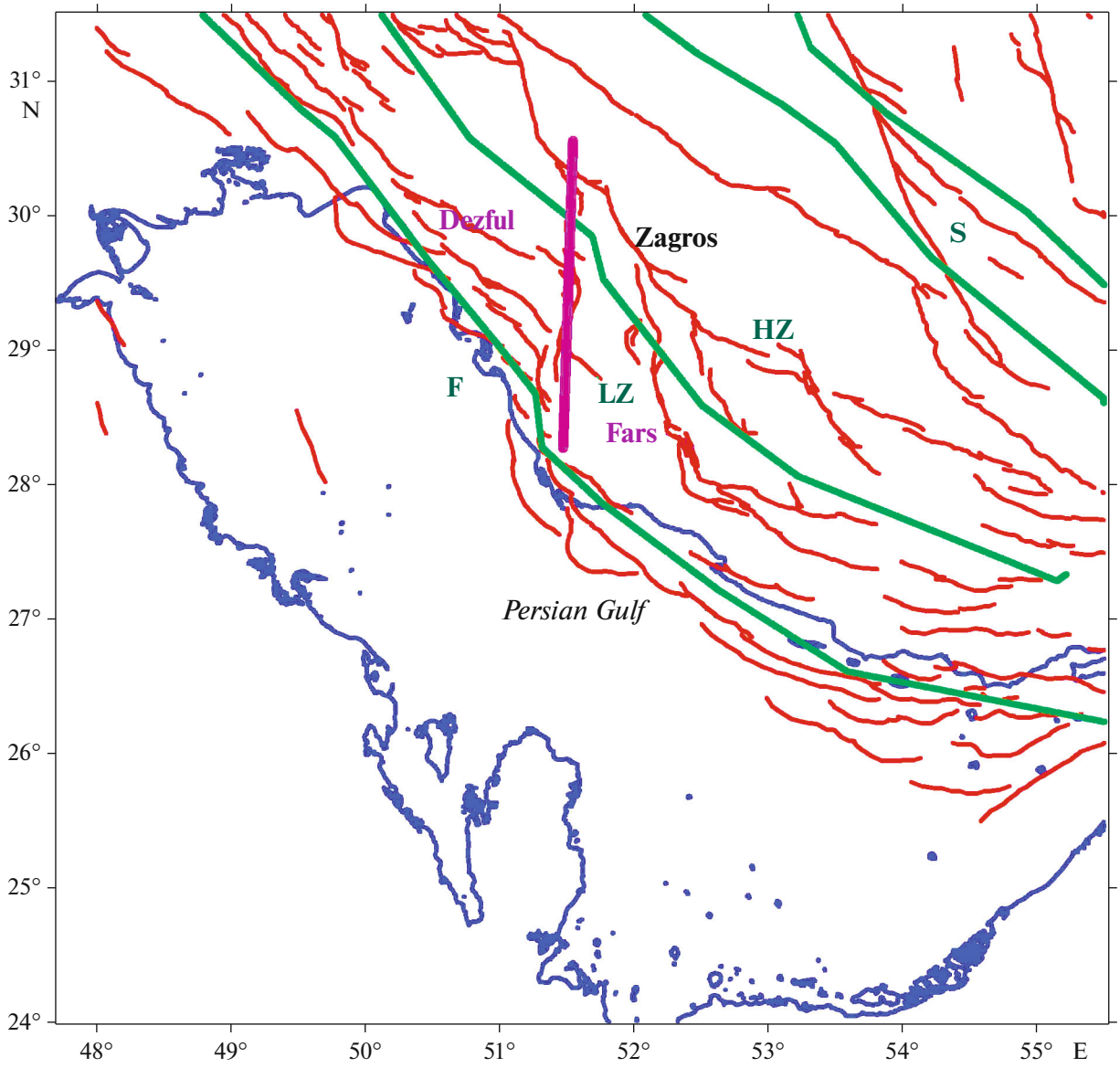

Fig. 1. Elements of tectonics of Persian Gulf and Zagros Mountains according to data [1, 2]. Red lines, faults; P, Piedmont zone; LZ, Low Zagros zone; HZ, High Zagros zone; I, Imbricated zone; purple line, Kazerun fault zone; green lines, boundaries of tectonic zones; Fars and Dezful, tectonic provinces.

Geophysical fields of the Persian Gulf and Crust of the Region

The thickness of the crust, according to model studies performed in [39], is about 40 km, increasing under the Zagros Mountains to 60 km.

The heat flow in the water area of the Persian Gulf, according to [47], reaches a value of about 55 mW/m^2, increasing up to 60 mW/m^2 under the Zagros Mountains. The gravity Bouguer and free air anomalies are close to zero; in the water area of the gulf, they do not exceed –20 mGal, but in the area of the Zagros Mountains, the free air anomalies increase to zero and Bouguer anomalies decrease to –200 mGal or less [32, 52].

Deviation from the geoid in the Persian Gulf water area is no greater than –13 m, increasing near the Zagros Mountains to a maximum of 13 m [44].

Magnetic field anomalies in the Persian Gulf are local in nature and have small amplitudes (no more than 70 nT) [53].

Modeling of the structure of the crust in the Persian Gulf in [39] on based on gravimetric data, information on the heat flow, the relief of the region, and deviations from the geoid, showed that the four-layer model of the crust is the most reliable. The model consists of a sediment layer with a thickness of 10 km and a density of 2530 g/cm^3; upper crust with a thickness of about 5 km and density of 2800 g/cm^3; middle

Table 1. Velocity sections of crust of Persian Gulf and Zagros Mountains

Link to data source	[39]		[16]	[41]	[21]			[34]			DSS		
layer	*d*	*h*	*V*	*V*	*d*	*h*	*V*	*d*	*h*	*V*	*d*	*h*	*V*
Sediments	10	10	5.3	5.0	3	3	4.0	7	7	5.5	5.0	5.0	4.1
Upper crust	15	5	6.0	6.3	13	10	5.5	15	8	6.2	4.5	4.5	6.0
Middle crust	23	8	6.1	6.4	20	7	6.0				21	11	6.3
Lower crust	40	17	6.5	6.9	45	25	6.7	42	27	6.5	40.5	20.0	6.8
Mantle							8.1						8.05

d is the depth of the base of the layer, km; *h* is the thickness of the layer, km; *V* is the average velocity in the layer, km/s.

crust with a thickness of 8 km and 2820 g/cm^3; and lower crust with a thickness of 17 km and density of 2950 g/cm^3. Then, according to [16], it is possible (rather conditionally) to estimate the velocity of longitudinal seismic waves in the crust of the Persian Gulf using the formula

$$\rho = 2\ln V_p - 0.8, \quad (1)$$

where ρ is the density of crustal rock in t/m^3 and V_p is the longitudinal seismic wave velocity in the layers of crust, km/s.

V_p in the upper layer (thickness 10 km), in accordance with modeling in [39], is 5.3 km/s (sediments); in the upper crust, V_p is close to 6 km/s (conditionally granitic rocks); in the middle crust (thickness 8 km), V_p is 6.1 km/s (conditionally granite rocks), in the lower crust (thickness 17 km), V_p = 6.5 km/s (conditionally basaltic rocks).

However, if we use the Neif-Drake plot [41, 42], then in the upper layer (thickness 10 km) V_p will be 5.0 km/s, in the upper crust (thickness 4 km) V_p = 6.3 km/s (conditional basalts), in the middle crust V_p = 6.4 km/s (conditional basalts) and in the lower crust V_p = 6.9 km/s (conditional basalts).

Paper [21] presents a velocity section of the crust obtained by processing records of three blasts recorded by seismic stations installed in the conjugation zone of the Fars and Dezful tectonic provinces (north of the Bushehr NPP (BNPP), Low Zagros zone) and used to localize microearthquakes in the study area. All of the above sections are summarized in Table 1.

The section from [21] significantly differs from that constructed from of modeling data [39] by a relatively thick (10 km) layer of sedimentary rocks with a velocity of 5.5 km/s and a layer of crystalline rocks (7 km) with a velocity of 6.3 km/s.

In [34], to construct the velocity section under the Persian Gulf water area, the arrival times of local seismic events were used, recorded by a dense seismological network. It was found that the velocity structure of the upper crust consists of a 7-km-thick sedimentary layer (where the P-wave velocity is 5.5 km/s) and an 8-km-thick upper crystalline crust (V_p = 6.2 km/s). This publication reports that an analysis of the records of seven teleseismic earthquakes suggests that the lower crust is 27 ± 2 km thick with a P-wave velocity of 6.5 km/s.

It should be noted that a brief review of publications on the structure of the crust in Persian Gulf water area indicates contradictory results. Use of different methods for reconstructing the velocity structure of a solid medium under the floor of the Persian Gulf: modeling based on gravimetric and other data [39]; interpretation of low-detail seismic data obtained from blasts [21], and reconstruction of the velocity structure from earthquake records [34] yield different crustal velocity sections. There are no publications on detailed seismic studies using deep seismic sounding (DSS) in the open press, which indicates the relevance of the research results presented in this article.

METHODS AND EQUIPMENT

To study the Persian Gulf water area, the following marine geophysics methods were used:

Deep seismic sounding (DSS) using refracted and reflected waves was carried out along three regional profiles, the method for which is described in [6]. Airguns (AG) with a total working chamber volume of 60 L and autonomous bottom seismographs (OBS) were used. The main marine profiles supplemented regional land profiles by other methods. Despite the difference in methods and apparatus, the marine and land data proved well-consistent. Thus, the general structure of the crust and sedimentary sequence of both the Persian Gulf and the construction site of the BNPP was obtained.

High-resolution 48-channel seismic profiling CDP (common depth point method) made it possible to study the structure of the sedimentary sequence and its velocity characteristics under the bottom of the Persian Gulf to a depth of about 1.0 km with a resolution of 1–2 m and to identify a number of acoustic inhomogeneities (listostromes, steep folds, gas saturation, faults, dislocations, etc.). The CDP results were used to construct regional depth profiles.

Super-resolution seismoacoustic profiling using a CHIRP-II seismic profiler (CAP-6600) was carried out to study the fine structure of the upper sediment

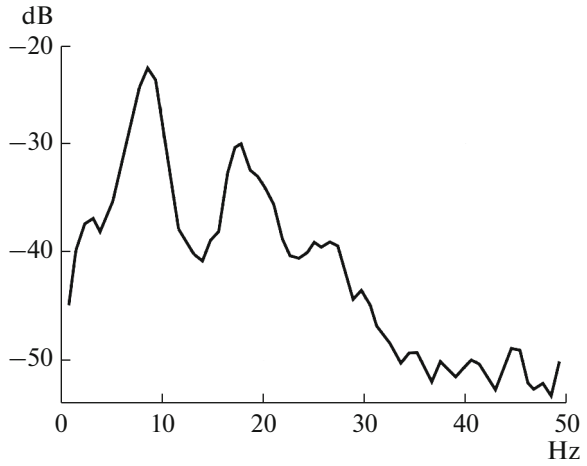

Fig. 2. Spectrum of airgun pulse, determined from data of control hydrophone record.

layer at a depth of 20–40 m below the seabed with a resolution of 10–30 cm in order to identify surface neotectonic faults, gas-saturated sediments, and gas seeps.

A local seismicity study using highly sensitive autonomous bottom seismological stations was carried out to determine the degree of activity of neotectonic faults at the bottom of the Persian Gulf.

In this article, due to the limited volume of the publication, only the results of works carried out by the DSS method are presented. In an abbreviated form, they are considered in [11], and the results of seismological observations–in [12].

Navigational support and positioning of the vessel (R/V *Professor Shtokman*) on the profiles, as well as during the mooring and raising of the bottom seismographs, was carried out using the DGPS global satellite navigation system. An NT300D satellite navigation receiver (Trimble Navigation) and dKart Navigator software system based on an electronic map were used.

DSS and Persian Gulf microearthquake studies used bottom seismographs developed jointly by IO RAS and the Joint Institute of Physics of the Earth RAS (JIPE RAS) [8, 23]. Each device recorded signals using an SV-5 type vertical seismic receiver with an eigenfrequency of 5 Hz. Additionally, the IO RAS instruments were equipped with hydrophones and SV-5M horizontal geophones. Signals from each sensor after amplification were continuously recorded on magnetic tape by direct recording with high-frequency bias. Each signal was recorded at two amplitude levels: rough and sensitive. The amplification of signals at each level differed by a factor of 10–25. The OBS used six information recording tracks and two service tracks, on which the pilot signal and time stamps were recorded. The frequency range of the record was 3–30 Hz at a level of 0.76, and the total dynamic range of the record was 60–75 dB at two amplitude levels. The recording duration varied from 5 to 14 days and depended on the speed of the magnetic tape, determined by the problem being solved. In the DSS studies, the recording time was calculated according to the total time to process one profile: from setting the OBS and shooting to the raising of the OBS to the surface. The accuracy of the quartz clock was 0.02 s per 10 days. Recording was determined by the stability of the reference quartz oscillator used in the OBS clock with a value of 2×10^{-8} s/day.

The seismograph was placed in a robust housing with a submerged weight of 40 to 100 kg for various modifications and was moored on the bottom with a nylon halyard 12 mm in diameter. Following the robust casing, 60 m of a nylon halyard was paid out overboard, to the other end of which a chain with a ballast weight of 70–100 kg was attached. The main buoy extended from the ballast weight, the free end of which was attached to the released surface buoy. All operations for mooring and raising the buoys were done with a winch, A-frame, and a crane. Between the seismograph lying on the bottom and the ballast weight holding the buoy, there was a halyard coupling, which isolated the seismograph from the influence of the surface buoy.

The OBS recording playback system was based of an eight-channel modified N-067 magnetograph. The playback speed exceeded the recording speed by 80–200 times, which transposed the seismic frequency range (3–30 Hz) into the acoustic frequency range (240–6000 Hz). Seismic signals recorded on the bottom became audible. With headphones connected to the playback system, records of AG signals and natural earthquakes were found ear.

An IBM PC with a multiplex 12-bit ADC was used to digitize the analog OBS records. The digitized record was visualized on the monitor and referenced to absolute UTC time. TFSA diagrams made it possible to estimate the evolution of the seismic signal spectrum over time in order to select the optimal filtering for more thorough processing. The amplitude and energy spectrum of the selected fragment of the record was calculated taking into account the frequency response of the seismometric channel of the OBS.

In the case of seismic events, fragments of earthquake records were saved. In the case of DSS studies, CSP traces were stacked.

Two PI-5 airguns with a volume of 30 L each were used for shooting [22, 25]. At shallow sea depths from 10 to 20 m, one AG worked at a depth of 7 m. The shooting interval was 60 s (1 min) or, at an average ship speed of 3 knots, about 90 m. At depths greater than 20 m, the second AG was put overboard and both guns were towed at a depth of 18 m. The shooting interval was 120 s (2 min) or an average of 180 m. To reduce the seismic signal excitation, shooting was also carried out in the opposite direction with an interval offset of 90 m. Thus, in the end, the traces on the profile had a 90 m interval.

Figure 2 shows the spectrum of the AG pulse, calculated from the data obtained by the control hydrophone.

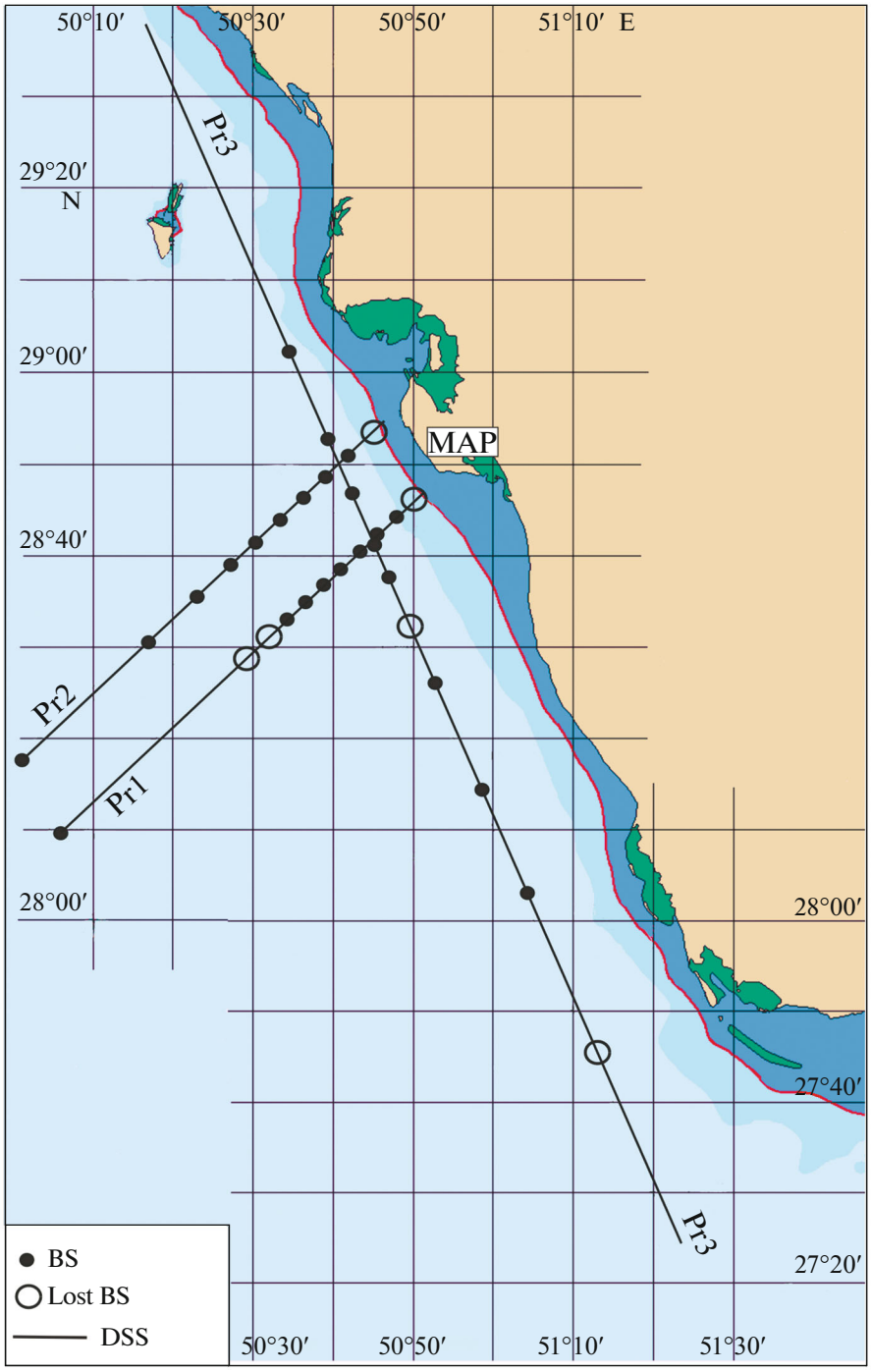

Fig. 3. DSS profiles. Black circles, position of OBSs; circles, locations of lost OBS or OBS that yield no records due to technical reasons.

To fire the AGs and synchronize the BS clocks, the following were used: an onboard accurate time system, consisting of a reference clock, a radio receiver of precision time signals, control clocks, hydrophone-markers of the times of AG emission, an AG control panel, an ADC board, and an IBM PC. It was used in two modes: (1) checking the BS clocks with the exact time prior to mooring and after raising, (2) in the AG fire control mode.

Methodology for Offshore DSS Studies

DSS studies of the crust of the Persian Gulf were carried out along three main profiles, shown in Fig. 3. The length of the profiles was 100 km for the lines perpendicular to the coast and 250 km for the line parallel to the coast.

The OBS offset was uneven and varied from 5 to 40 km. Reducing the offset depended on a priori geo-

logical information to obtain more reliable material in areas with a complex structure. Information was not obtained from all buoys, due to their by local fishermen (four OBS) or equipment failure (three OBS).

During the work on the GSS in Persian Gulf water area, the IO RAS coastal team installed found land-based seismic stations: three at the construction sight of the BNPP and one in Bushehr to record AG signals on land in order to obtain data on the velocity structure of the crust directly under the Bushehr Peninsula. Unfortunately, no AG signals were found in the coastal station records due to the strong technogenic seismic background.

Processing and Interpretation of DSS data

During preprocessing of then field data, the CSP records were created as SEGY files [28]. Processing included the following:

— Digitization of analog records from bottom and coastal seismic stations.

— Formation of a database of field observations and the creation of an archive on various external media.

— Creation of CSP stacks based on data of the AG shooting time as SEGY format files.

— Calculation and entry in the trace headers of the offsets and distance along the profile.

— Absolute GMT referencing of each seismic trace.

— Introduction of static time corrections.

— All available information was also recorded in the headers in accordance with the SEGY standard.

Quality control of records was done by viewing the stacks on the monitor. As well, defective traces were rejected and the correctness of the stacking was checked against the arrival time of the reflected wave from the bottom. As an example of a CSP record, Fig. 4 shows two CSP stacks for the third profile.

When interpreting the DSS data and constructing deep velocity sections, the following procedures were performed:

— Frequency and τ–p filtering of subcritical reflected waves.

— Picking of target waves and construction of systems of the opposite and overtaking travel time curves with subsequent time referencing at cross points.

— Solution of the one-dimensional inverse problem (1D inversion).

— Solution of the two-dimensional inverse problem (2D inversion).

— Construction of a two-dimensional deep velocity section, taking into account the data of the two inversion methods and a priori geological data.

— Optimization of a two-dimensional depth velocity model by solving the direct kinematic problem for complex media.

Processing of DSS seismic data, interpretation, and construction of deep 2-D velocity models will be illustrated with profile 3, the most informative for studying the structure of the crust.

The one-dimensional inverse problem was solved under the assumption of plane-parallel boundaries V.Yu. Burmin's method and software [4, 5]. Inversion was carried out for the travel time curves of refracted waves. The horizontal homogeneity of the model results in different inversion results for the left and right branches of the hodographs. Examples of results are given in Fig. 5 in the form of stacked velocity columns for the right and left branches.

The travel time curves of refracted waves were processed and interpreted using V.B. Piip's method of homogeneous functions [17, 19, 20, 45, 46].

The used HODOGRAPH software package automatically interprets the refracted wave travel times for complex media in conditions where horizontal and vertical velocity can vary significantly. The method does not require a priori information, and the operation of identifying waves on the first arrival travel time curves is done automatically.

The calculated depth sections (Fig. 6) represent the velocity field specified at the nodes of a rectangular grid. This field contains information about interfaces and faults. The inversion interfaces (velocity decreases abruptly from top to bottom) look like thickened lines and are aligned with the field of velocity isolines (Fig. 6). Velocity values on sections within layers and blocks always increase from top to bottom.

The two-dimensional (2D) depth velocity model was constructed as follows:

The velocity in the sedimentary sequence and interfaces were taken from the CDP model for the third profile. Sites were placed on the depth model in accordance with the location of the critical point for each boundary along the left and right branches according to the 1D inversion data. The velocity under the site was determined by the corresponding speed column. Refracting boundaries and velocities were constructed based on 2D inversion and referenced to the 1D inversion site.

The constructed sections were refined by solving the two-dimensional (2D) direct problem by the selection method by formalizing inhomogeneous velocity models and associated numerical solution of the direct kinematic Zelt problem [50, 51]. In this case, the graphics shell SeisWide was used (author Deping Chain [54]), where the experimental and theoretical travel time curves were compared.

Figure 7 depicts estimation of the accuracy in comparing the experimental and theoretical travel time curves. Figure 7b shows that, in general, the discrepancy between the observed and theoretical hodographs for profile model 3 does not exceed ± 0.1 s.

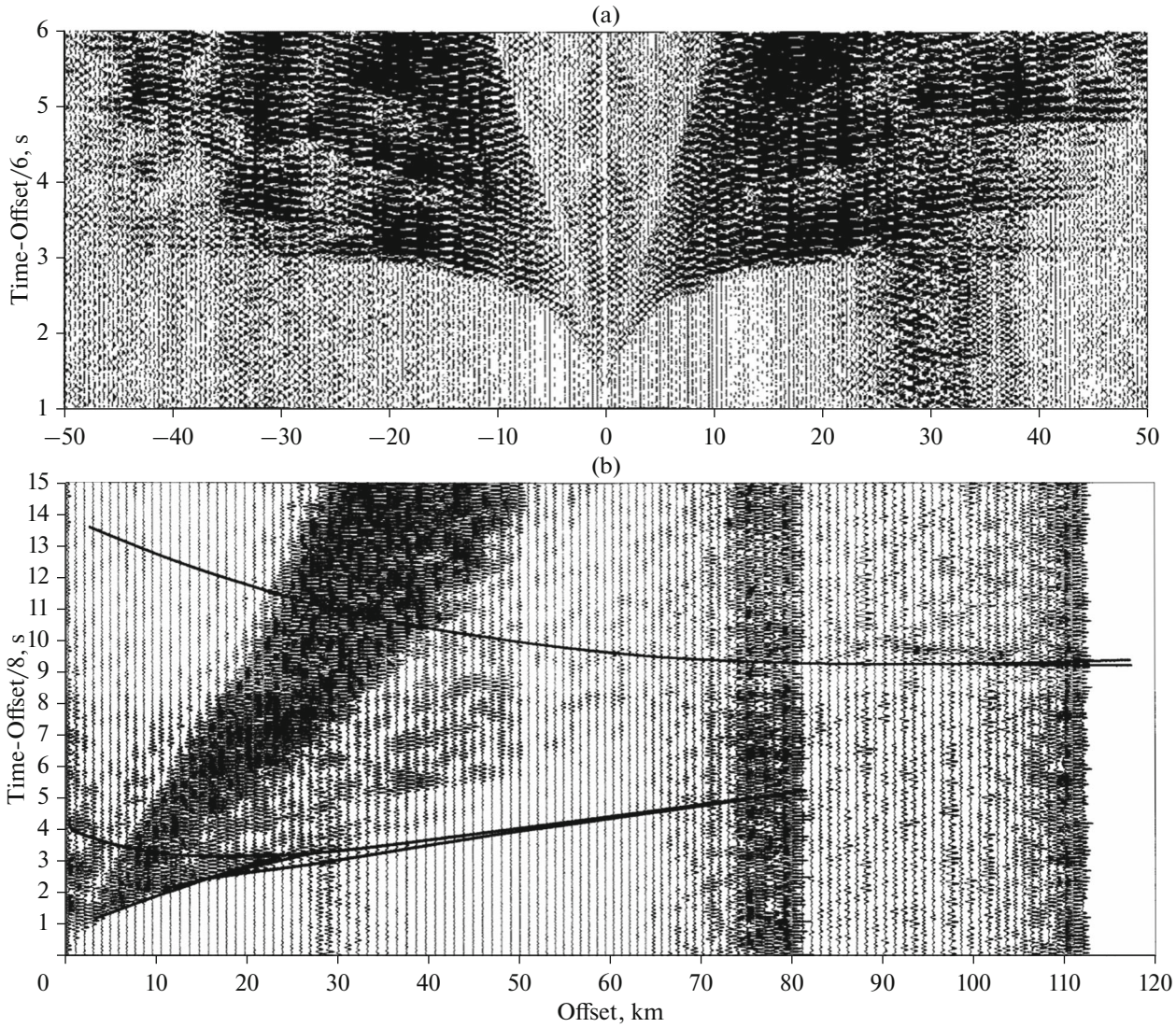

Fig. 4. Examples of CSP stacks of hydrophone for profile 3: (a) in 6 km/s reduction; (b) in 8 km/s reduction.

The deep velocity section obtained using the Zelt program for profile 3 is shown in Fig. 8.

Similarly, deep velocity sections were constructed for profiles 1 and 2 (Figs. 9a, 9b, respectively). Due to the large distance between OBS 9 and OBS 10 on profile 2, there was not enough information to reliably interpret this part of the section at depths of up to 1–1.5 km, but the deeper layers of the section were interpreted quite reliably.

Comparison of velocity sections for all three profiles shows that the most complex structure is at the intersections of profiles 1 and 2 with profile 3. On profile, a zone with a complex structure was found, located at a distance interval of 90–180 km along profile 3. Profile 2 crosses this zone at the 96th km, and profile 1, at the 110th km of profile 3. Here, there is a correlation of dome-shaped structures at the points of setting OBS 6–8, profile 1; 3–5, profile 2; and 6–8, profile 3.

The structure revealed on profiles 1–3 is possibly a brachyanticline with an isometric dome shape, which corresponds to platform-type folding in salt-dome tectonic zones. The typical dimensions of this structure are 10 × 20 km and are similar in size to the Bushehr anticline.

DISCUSSION

Due to the coastal location of the profiles, where the quality of the recording is strongly influenced by the surf and technogenic noise, the majority of first arrivals on the seismograms were traced at distances no greater than 35 km from the OBS. This prevents constructing velocity models deeper than 6–7 km (Figs. 8, 9) based on the set of refracted and reflected waves.

Refracted waves with apparent velocities of 5.8–6.4 km/s were recorded in first arrivals up to maxi-

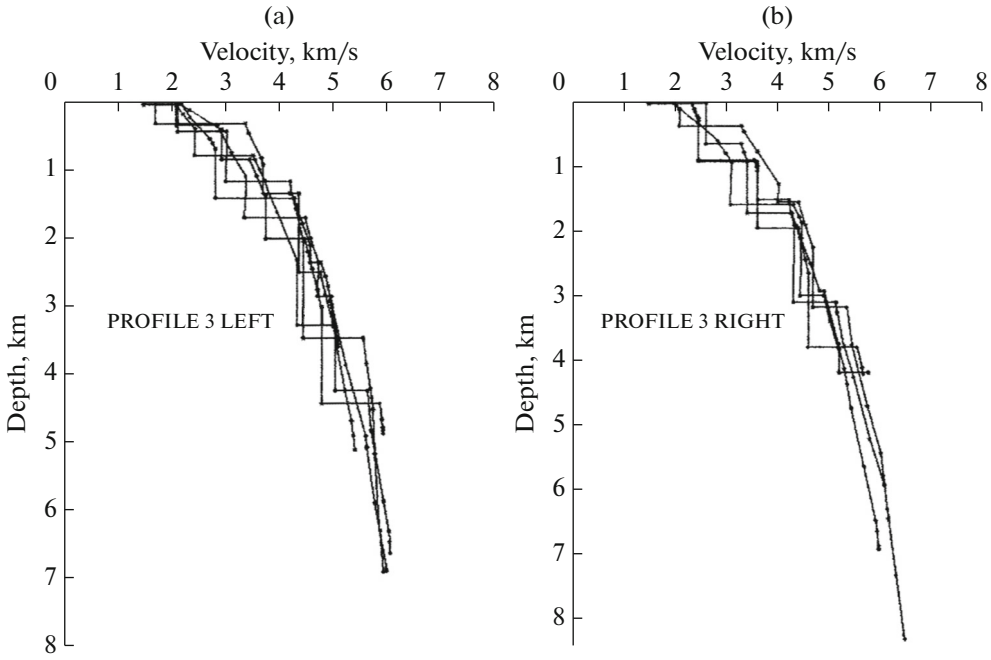

Fig. 5. Combined velocity columns for profile 3: (a) to left of OBS, (b) to right of OBS.

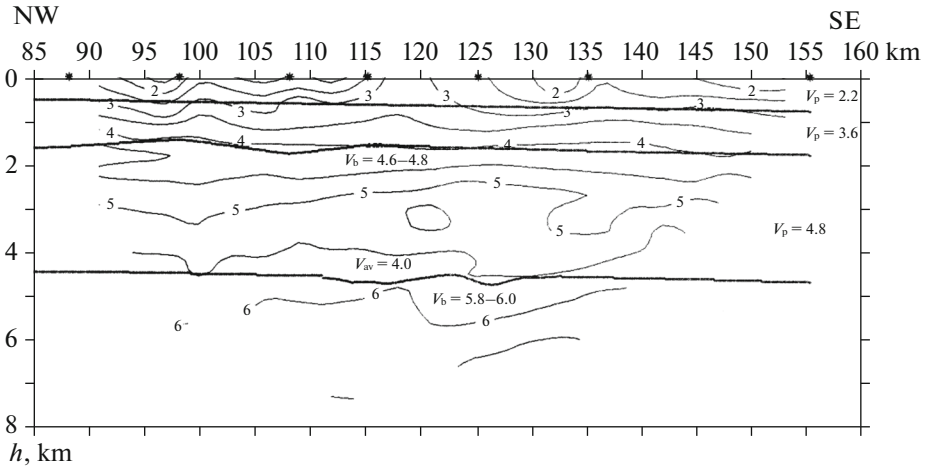

Fig. 6. Deep velocity section along profile 3, constructed by homogeneous functions method. Asterisks on exposed surface, position of OBS; thick solid lines, boundaries of the first kind; V_{av}, average interval velocity in km/s; V_b, value of boundary velocity in km/s; numerals on isolines, velocity in km/s.

mum distances of 45–50 km. This corresponds to penetration of seismic rays of refracted waves to maximum depths of 6–8 km. At great depths, there is a sharp increase in the absorption of longitudinal seismic waves, distinctly seen on the combined seismogram shown in Fig. 4b. At the same time, the contrasting boundary corresponding to the foot of the basement according to the DSS data is well marked by a velocity jump of 5.1/5.9 km/s at a depth of 6 km.

However, in the seismic records, reflected waves from deeper boundaries were clearly present.

In the records of some OBSs, low-intensity reflected waves are recorded at times of 6–12 s. The reflected wave appears in the "double" time interval of 4.8 s, which corresponds to a boundary depth of 9.9 km at V_{av} = 4.1 km/s. On profiles 1, 2, 3, subcritical reflections were recorded at time intervals corresponding to boundary depths from 9 to 11 km. This boundary can be interpreted as the base of the upper crust.

Figure 4b shows the combined seismogram constructed from the OBS-9 records on profile 3 in the

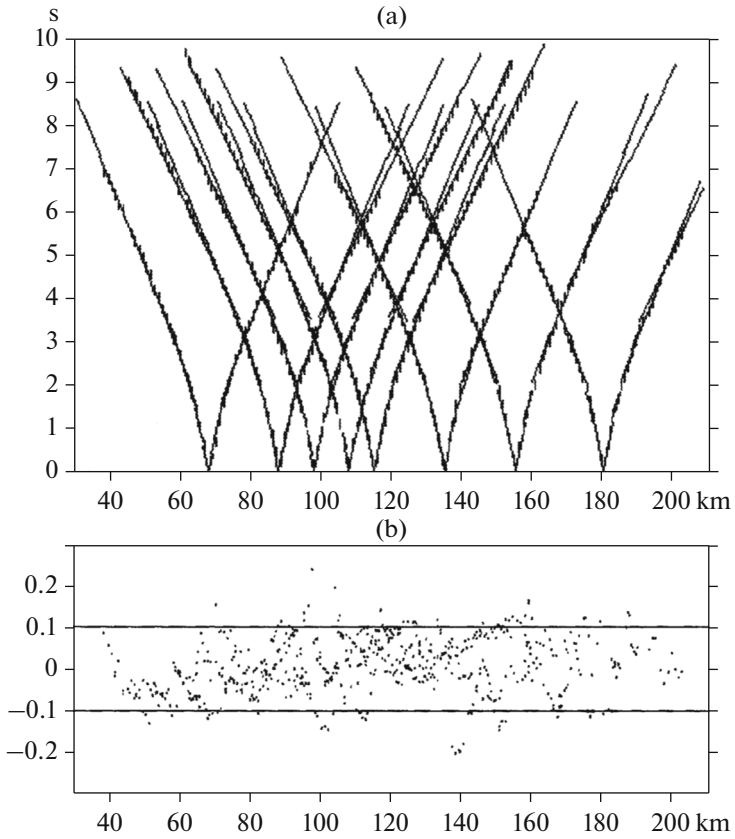

Fig. 7. Comparison of experimental and calculated hodographs for profile 3: top (a), vertical strokes | are experimental picking points (size of stroke corresponds to picking accuracy of 0.1 s); solid lines are calculated travel time curves; bottom (b) shows difference between calculated and observed travel times of seismic waves depending on distance along profile.

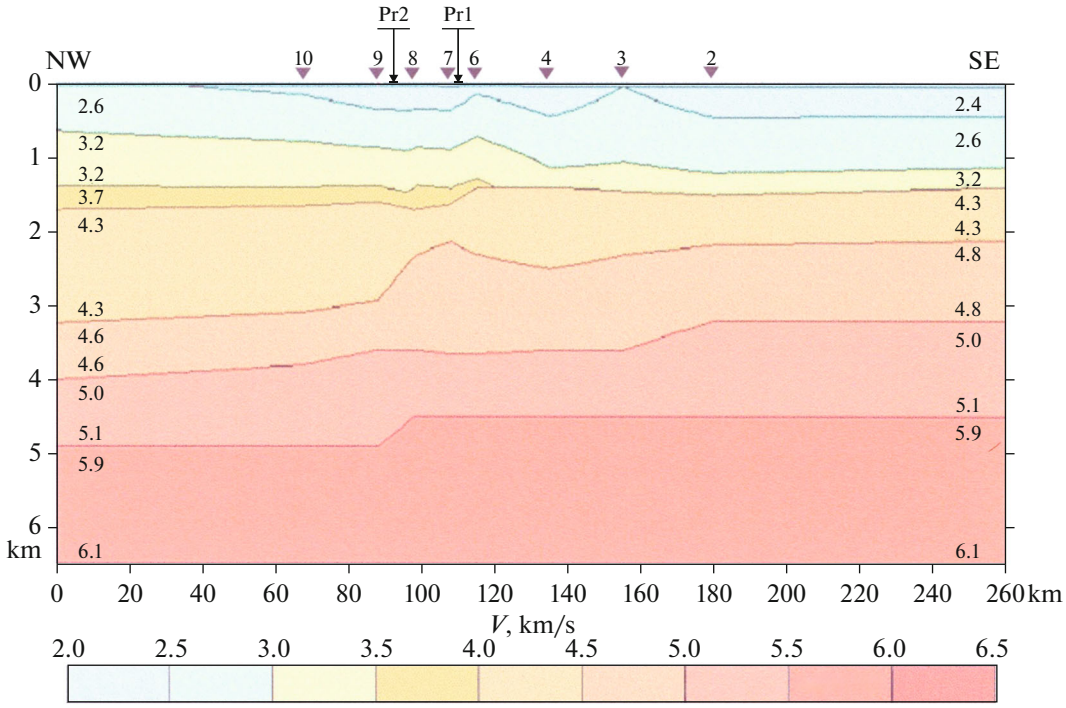

Fig. 8. Deep velocity profile section 3. Numerals at interfaces indicate velocity in km/s. Triangles on exposed surface, positions of OBSs. Arrows, intersections with profiles 1 and 2.

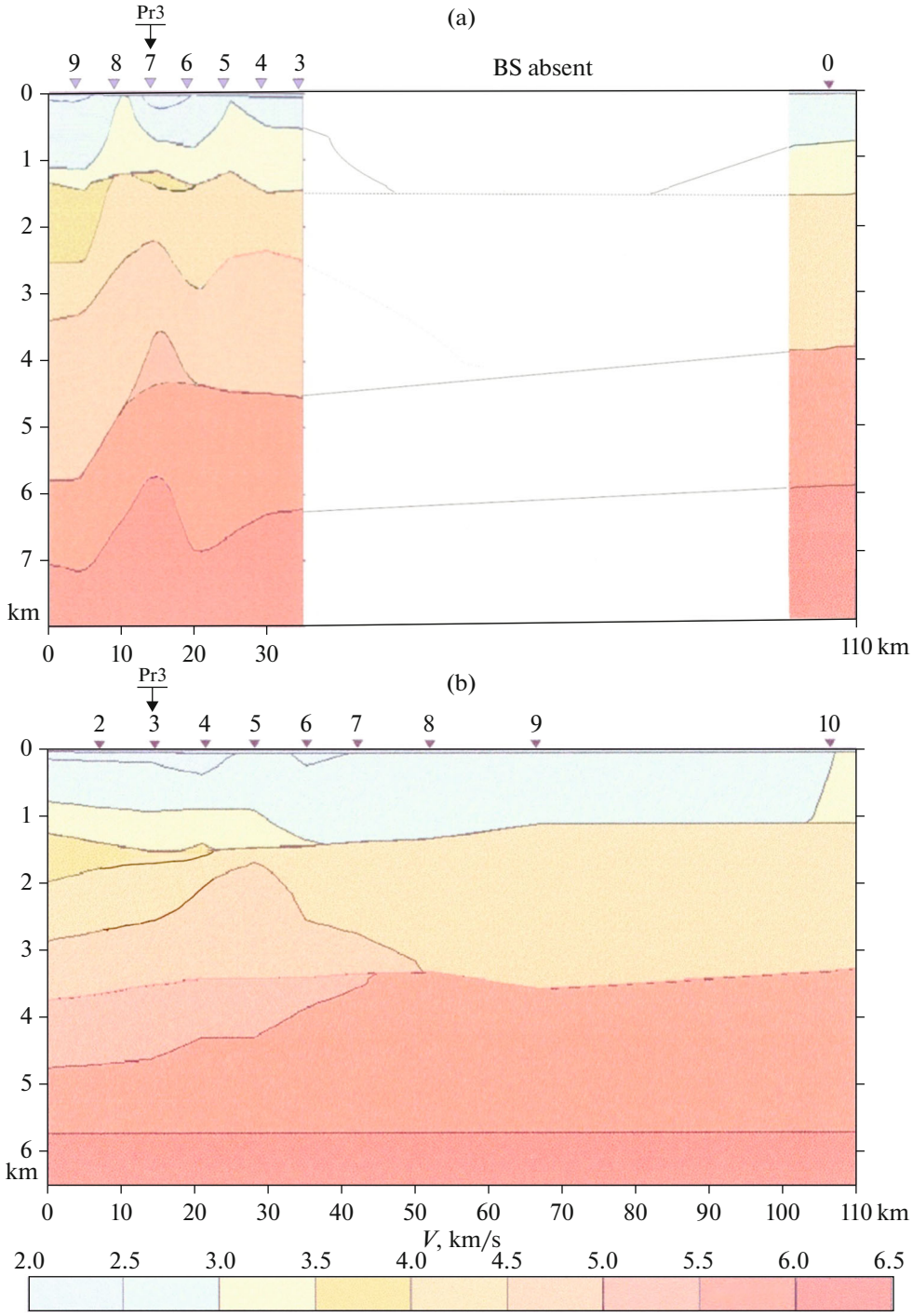

Fig. 9. Deep velocity sections of profiles 1 and 2. Numerals at interfaces, velocity in km/s. Triangles on exposed surface, positions of OBSs. Arrows, intersection with profile 3. (a) Profile 1, white space on section, no data (see text for explanation); (b) profile 2.

velocity reduction $V = 8$ km/s. On the seismogram at distances of 85–105 km, a supercritical reflection of a longitudinal seismic wave from the Moho surface is distinguished.

Kinematic modeling yielded the estimated position of the surface of the Moho of 37–41 km with inclination towards the beginning of profile 3. Modeling was performed by the fitting method; it was assumed that the velocity in the crust from its top to the Moho boundary varies linearly from 6.2 km/s at its top to 6.8 km/s at its bottom. During modeling, it was possible to identify an intermediate refractive boundary at a depth of 20 km. Figure 10 shows the depth velocity model of profile 3 with simplified boundaries below the basement.

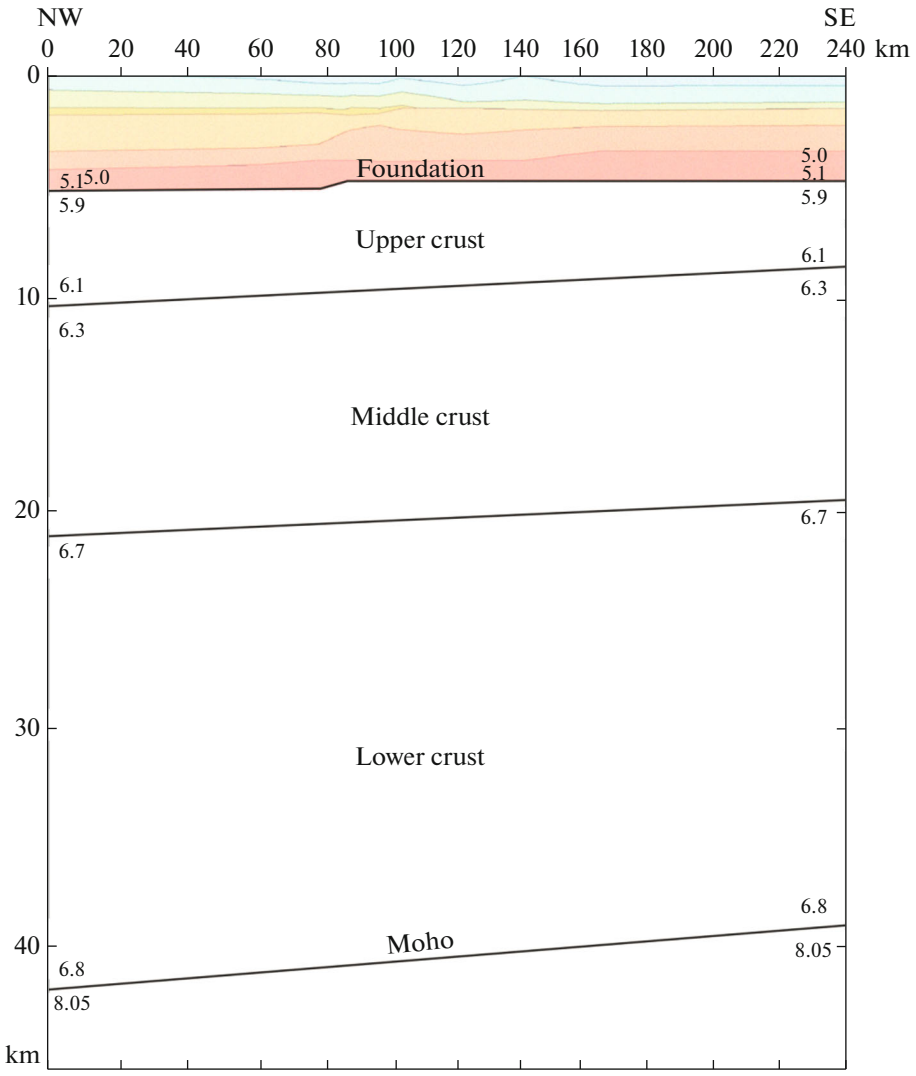

Fig. 10. Estimated of position of basement and Moho boundary.

As a result of DSS studies using OBSs and large-volume airguns, a velocity section of the crust was obtained in the Persian Gulf water area to a depth of 40–43 km. Previously, such information was not available in the open press.

The velocity section is represented by the following layers (from top to bottom):

Layer 1 with V_p = 2.0–5.1 km/s (average velocity 4.1 km/s) and thickness of 5 km (the top of the layer is located at a depth of 0 km; the bottom was determined at a depth of 5 km). Apparently, this layer consists of sedimentary rocks.

Layer 2 with V_p = 5.9–6.1 km/s and a thickness of 4 to 5 km. The top of the layer is located at a depth of 5 km. It was interpreted by us as the roof of the crystalline basement. The bottom of the layer rises gradually from northwest to southeast from a depth of 10.5 km to about 8 km. The rocks making up this layer can apparently be attributed to conditional granites.

Layer 3 with V_p = 6.3 km/s and a thickness of about 11 km. The top of the layer is located at a depth of 10.5 km in the northwest of the study area and gradually rises to a depth of 8 km in the southeast. The base of the layer also rises from a depth of about 21.5 km in the northwest to a depth of 19.5 km in the southeast. This layer can be interpreted as the middle crust.

Layer 4 with V_p = 6.7–6.8 km/s and a thickness of about 20 km. The top of the layer is located at a depth of 21 km in the northwest of the study area and gradually rises to a depth of 19.5 km in the southeast. The base of the layer also rises from a depth of about 42 km in the northwest to 39 km in the southeast. This layer can be interpreted as the lower crust, and its base can be taken as the Moho boundary.

The possibility of uplifted interfaces in the crust of the Persian Gulf during the transition from the Dezful to the Fars province is noted in [3]. This effect has been substantiated here by geological methods. It is

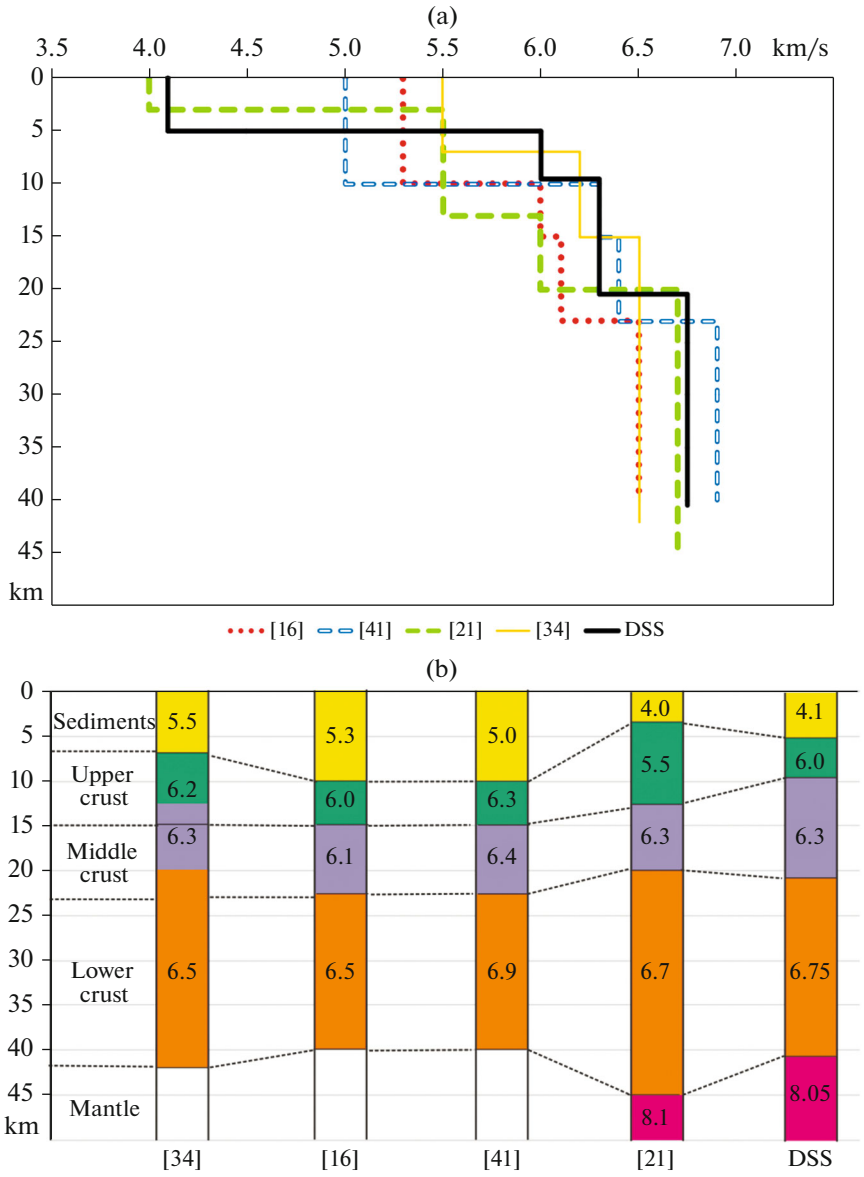

Fig. 11. Velocity models of crust of Persian Gulf: (a) change in seismic wave velocity as function of depth; (b) in form of 1D seismic sections. Numerals in square brackets are a link to source of model; DSS, model constructed according to data of section in Fig. 10.

noted in [24] that the crust becomes more mafic in this case.

CONCLUSIONS

The closest to the obtained section is the velocity model of the medium obtained from modeling based on gravimetric and other data [39], in which the rock densities are recalculated to compressional wave velocities using the Nafe–Drake relation [41]. Figure 11 shows the parameters of the models under consideration.

The main discrepancy between the models is observed in the sedimentary cover, where the P-seismic wave velocities are 4.1 km/s according to the DSS data and 5 km/s according to the modeling data. In addition, the thickness of sediments in the Nafe–Drake model is 10 km, while according to the DSS data, it is 5 km. Interval velocities in other layers of the crust are nearly the same in both models. The depths of the Moho boundaries and the tops of the lower crust are also very close in them.

It should also be noted that the DSS method, where seismic wave travel velocities are measured, is a more accurate tool for constructing velocity sections of the crust compared to calculation methods that model velocity parameters in the layers of the crust based on geophysical data.

All the considered models and the obtained section of the crust by the DSS method indicate that in the

crust under Persian Gulf water area, the layer of conditionally granitic rocks has a reduced thickness (about 4–5 km).

Thus, the crust of the Persian Gulf, following the generalizations presented in [9, 10, 40], can be attributed to Archean subcontinental crust. Such a situation (complete absence or thinning of the upper layer of the crust) is typical of water areas closest to the Persian Gulf: the Black [7, 13–15, 18], Caspian [20], Mediterranean [38], and Red [33] seas.

The DSS data show that there are no faults in the crust within a radius of 100 km from the construction site of the Bushehr nuclear power plant.

As a result of the studies, a structure was discovered in the crust of the study area, possibly, is a brachyanticline, which has an isometric dome shape corresponding to platform-type folding in salt-dome tectonic zones. The typical dimensions of this structure are 10 × 20 km and are similar in size to the Bushehr anticline.

FUNDING

The study was carried out within the state task of IO RAS (topic no. FMWE-2021-0004) and was supported by the Russian Foundation for Basic Research (project no. 20-77-00034).

REFERENCES

1. Kh. M. D. Aldzhabasini, Candidate's Dissertation in Geology and Mineralogy (Geol. Inst. Ross. Akad. Nauk, Moscow, 2021).
2. Active Faults of Eurasia Database (AFEAD).Geological Institute of the Russian Academy of Sciences. Laboratory of Neotectonics and Recent Geodynamics. http://neotec.ginras.ru/database.html.
3. D. M. Bachmanov, Extended Abstract of Candidate's Dissertation in Geology and Mineralogy (Geol. Inst. Ross. Akad. Nauk, Moscow, 2002).
4. V. Yu. Burmin, "Inversion of the common-reflection-point travel-time curve for a vertically inhomogeneous medium with a curvilinear boundary,"Dokl. Ross. Akad. Nauk **342** (3), 386–389 (1995).
5. V. Yu. Burmin, "Inversion of a discontinuous travel-time curve of refracted wave,"Dokl. Ross. Akad. Nauk **337** (4), 521–524 (1994).
6. B. N. Grin'ko, S. A. Kovachev, and A. V. Khortov, "Structure of the ShatskyRise (Black Sea) based on the results of regional seismic surveys of refraction,"Byull. MOIP. Otd. Geol. **79** (3), 3 (2004).
7. N. V. Esin, A. V. Khortov, and N. I. Esin, "On the mechanism of formation of "graniteless" basins of the Black Sea," EkologiyaGidrosfery **1** (6), 28–39 (2021).
8. S. M. Zverev, G. N. Akimov, V. S. Novikov, et al., "Equipment for deep seismic sounding and study of local earthquakes on land and at sea,"Seism. Pribory, No. 11, 75–77 (1978).
9. S. N. Kashubin, N. I. Pavlenkova, O. V. Petrov, et al., "Types of the Earth's crust in the circumpolar Arctic, Region. Geol. Metallogen., No. 55, 5–20 (2013).
10. S. N. Kashubin, O. V. Petrov, E. D. Mil'shtein, et al., "Types of the Earth's crust in Central and Northeast Asia, Far Eastern and Arctic regions of the continent–ocean transition," Region. Geol. Metallogen, No. 73, 6–18 (2018).
11. S. A. Kovachev, A. A. Krylov, O. Yu. Ganzha, and A. V. Egorov, "Deep seismic sounding of the Earth's crust in the waters of the Persian Gulf,"in *Modern Methods and Means of Oceanological Research (MSOI-2021). Proc. XVII Int. Sci. Tech. Conf.* (Inst. Okeanol. Ross. Akad. Nauk, Moscow, 2021), pp. 205–208.
12. S. A. Kovachev, A. A. Krylov, and A. V. Egorov, "Results of bottom seismological observations in the waters of the Persian Gulf," in *Modern Methods and Means of Oceanological Research (MSOI-2021). Proc. XVII Int. Sci. Tech. Conf.* (Inst. Okeanol. Ross. Akad. Nauk, Moscow, 2021), pp. 201–204.
13. M. V. Muratov and S. I. Subbotin, "Conclusion," in *The Earth's Crust and the History of the Development of the Black Sea Depression* (Nauka, Moscow, 1975), pp. 329–331.
14. Yu. P. Neprochnov, "Deep structure of the Earth's crust under the Black Sea according to seismic data," Byull. MOIP. Otd. Geol. **35**, 30–35 (1960).
15. Yu. P. Neprochnov, V. P. Goncharov, and A. F. Neprochnova, "Seismic data on the structure of the Earth's crust in the central part of the Black Sea," Dokl. Akad. Nauk SSSR **129** (2), 408–411 (1959).
16. *Petrophysics: Reference Guide in Three Books. Book 1. Rocks and Minerals*, Ed. by N. B. Dortman (Nedra, Moscow, 1992) [in Russian].
17. V. B. Piip, "Local reconstruction of a seismic section from refracted wave data based on homogeneous functions," FizikaZemli, No. 10, 24–32 (1991).
18. V. B. Piip and A. P. Ermakov, "Oceanic crust of the Black Sea basin according to seismic data," Vestn. Mosk. Univ. Ser. 4. Geol., No. 5, 61–68 (2011).
19. V. B. Piip and A. G. Rodnikov, "Deep structures of the continental margin of Primorye–Sea of Japan according to seismic data,"Vestn. Mosk. Univ. Ser. 4. Geol., No. 2, 61–67 (2009).
20. V. B. Piip, A. G. Rodnikov, and N. A. Buvaev, "Study of the deep structure of the lithosphere along the seismic profile Caucasus–South Caspian depression–Absheron threshold–Middle Caspian depression–Turan plate," Vestn. Mosk. Univ. Ser. 4. Geol., No. 2, 45–51 (2012).
21. Yu. L. Rebetskii, A. A. Lukk, R. E. Tatevosyan, and V. V. Bykova, "Determination of weak earthquake focal mechanisms and modern geodynamics of Southern Iran," Geodyn. Tectonophys. **8** (4), 971–988 (2017).
22. *Seismic Exploration. Geophysicist's Handbook*, Ed. by I. I. Gurvich and V. P. Nomokonov (Nedra, Moscow, 1981) [in Russian].
23. S. L. Solov'ev, S. A. Kovachev, I. P. Kuzin, and E. V. Voronina, *Microseismicity of the Aegean and Tyrrhenian Seas According to the Observations of Bottom Seismographs* (Nauka, Moscow, 1993).

24. V. G. Trifonov, "Neotectonics of mobile belts,"Tr. Geol. Inst. (GEOS, Moscow, 2017).
25. V. K. Utnasin, Yu. A. Moskalenko, N. V. Badikov, et al., RF Patent 2034310 C1 (1995).
26. M. B. Allen, J. Jackson, and R. Walker, "Late Cenozoic reorganization of the Arabia–Eurasia collision and the comparison of short-term and long-term deformation rates," Tectonics **23** (2), TC2008 (2004).
27. M. B. Allen, C. Saville, and E. J.-P. Blanc, et al., "Orogenic plateau growth: Expansion of the Turkish-Iranian plateau across the Zagros fold-and-thrust belt," Tectonics **32**, 1–20 (2013).
28. K. M. Barry, D. A. Cavers, and C. W. Kneale, "Recommended standards for digital tape formats," Geophysics **40** (2), 344–352 (1975).
29. M. Berberian and G. C. P. King, "Towards a paleo-geography and tectonic evolution of Iran," Can. J. Earth Sci. **18**, 210–265 (1981).
30. P. Bird, "Finite element modeling of lithosphere deformation: The Zagros collision orogeny," Tectonophysics **50**, 307–336 (1978).
31. P. Bird, Z. M. N. Tokso, and N. H. Sleep, "Thermal and mechanical models of continent-continent convergence zones," J. Geophys. Res. **32**, 4405–4416 (1975).
32. G. Dekhani and J. Makris, "The gravity field and crustal structure of Iran," NeuesJahrb. Geol. Paleontol. Abh. **168**, 182–207 (1988).
33. F. Egloff, R. Rihm, J. Makris, et al., "Contrasting structural styles of the eastern and western margins of the southern Red Sea: the 1988 SONNE Experiment," Tectonophysics **198**, 329–353 (1991).
34. D. Hattzfeld, M. Tatar, K. Priestley, and M. Ghafory-Astiany, "Seismological constraints on the crustal structure beneath the Zagros mountain belt (Iran)," Geophys. J. Int., No. 155, 403–410 (2003).
35. D. Hatzfeld and P. Molnar, "Comparisons of the kinematics and deep structures of the Zagros and Himalaya and of the Iranian and Tibetan plateaus and geodynamic implications," Rev. Geophys. **48**, Rg2005 (2010).
36. J. Jackson and D. McKenzie, "The relationship between plate motion and seismic moment tensors, and the rates of active deformation in the Mediterranean and Middle East," Geophys. J. R. Astron. Soc. **93**, 45–73 (1988).
37. J. Liu-Zeng, P. Tapponnier, Y. Gaudemer, and L. Ding, "Quantifying landscape differences across the Tibetan plateau: Implications for topographic relief evolution," J. Geophys. Res. **113**, F04018 (2008).
38. J. Makris and T. Yegorova, "A 3-D density–velocity model between the Cretan Sea and Libya," Tectonophysics **417**, 201–220 (2006).
39. S. H. Montavalli-Anbaran, H. Zeyen, M.-F. Brunet, and V. E. Ardestani, "Crustal and lithospheric structure of the Alborz Mountains, Iran, and surrounding areas from integrated geophysical modeling," Tectonics **30**, TC5013 (2011).
40. W. D. Mooney, "Crust and lithospheric structure—global crustal structure," in *Treatise on Geophysics*, Vol. 1: *Seismology and Structure of the Earth*, Ed. by B. Romanowicz and A. Dziewonski (Elsevier, Amsterdam, 2007), pp. 361–417.
41. J. Nafe and C. Drake, "Physical properties of marine sediments," in *The Sea* (Intersci. Publ., New York, 1963), Vol. 3.
42. A. Nakanishi, H. Shiobara, R. Hino, et al., "Detailed subduction structure across the eastern Nankai trough obtained from ocean bottom seismographic profiles," J. Geophys. Res. **103** (11), 27 151–27 168 (1998).
43. A. Paul, D. Hatzfeld, A. Kaviani, et al., "Seismic imaging of the lithospheric structure of the Zagros, *Geological Society* (Special Publications, London, 2010), Vol. 330, pp. 5–18.
44. S. A. Holmes, S. C. Kenyon, and J. K. Factor, "An Earth gravitational model to degree 2160: EGM2008," *General Assembly of the European Geosciences Union, Vienna, Austria* (April 13–18, 2008).
45. V. B. Piip, "2D Inversion of refraction traveltime curves using homogeneous functions," Geophys. Prosp. **49**, 461–482 (2001).
46. V. B. Piip and A. G. Rodnikov, "The Sea of Okhotsk crust from deep seismic sounding data," Russ. J. of Earth Sci. **6** (1), 1–14 (2004).
47. H. N. Pollac, S. J. Hurter, and J. R. Johnson, "Heat flow from the Earth's interior: Analysis of the global data set," Earth Planet Sci. Lett. **244** (1–2), 285–301 (1993).
48. A. M. C. Sengor and W. S. F. Kidd, "Post collisional tectonics of the Turkish-Iranian plateau and a comparison with Tibet," Tectonophysics **55**, 361–376 (1979).
49. V. G. Trifonov, "Zagros structure of the mountain belt (Iran)," *Geological Society* (Special Publications, London, 2010), Vol. 330, pp. 5–18.
50. C. A. Zelt, "Modelling strategies and model assessment for wide-angle seismic travel-time data," Geophys. J. Int., No. 139, 183–204 (1999).
51. C. A. Zelt and R. B. Smith, "Seismic travel-time inversion for 2-d crustal velocity structure," Geophys. J. Int., No. 108, 16–34 (1992).
52. Observatoire Midi-Pyrénées. https://bgi.omp.obs-mip.fr.
53. NOAA. EMAG2v3: Earth Magnetic Anomaly Grid. https://data.nodc.noaa.gov/cgi-bin/iso?id=gov.noaa.ngdc.mgg.geophysical_models:EMAG2_V3.
54. SeisWide 4.7. http://seismic.ocean.dal.ca/~seismic/utilities/seiswide/index.php.